



OPEN

## A time fractional model of a Maxwell nanofluid through a channel flow with applications in grease

Naveed Khan<sup>1</sup>, Farhad Ali<sup>1</sup>✉, Zubair Ahmad<sup>1</sup>, Saqib Murtaza<sup>1</sup>, Abdul Hamid Ganie<sup>2</sup>, Ilyas Khan<sup>3</sup> & Sayed M. Eldin<sup>4</sup>

Several scientists are interested in recent developments in nanotechnology and nanoscience. Grease is an essential component of many machines and engines because it helps keep them cool by reducing friction between their various elements. In sealed life applications including centralized lubrication systems, electrical motors, bearings, logging and mining machinery, truck wheel hubs, construction, landscaping, and gearboxes, greases are also utilized. Nanoparticles are added to convective grease to improve its cooling and lubricating properties. More specifically, the current study goal is to investigate open channel flow while taking grease into account as a Maxwell fluid with  $MoS_2$  nanoparticles suspended in it. The Caputo-Fabrizio time-fractional derivative is used to convert the issue from a linked classical order PDE to a local fractional model. To determine the precise solutions for the velocity, temperature, and concentration distributions, two integral transform techniques the finite Fourier sine and the Laplace transform technique are jointly utilized. The resultant answers are physically explored and displayed using various graphs. It is important to note that the fractional model, which offers a variety of integral curves, more accurately depicts the flow behavior than the classical model. Skin friction, the Nusselt number, and the Sherwood number are engineering-related numbers that are quantitatively determined and displayed in tabular form. It is determined that adding  $MoS_2$  nanoparticles to grease causes a 19.1146% increase in heat transmission and a 2.5122% decrease in mass transfer. The results obtained in this work are compared with published literature for the accuracy purpose.

Both Newtonian and non-Newtonian fluids are prevalent in nature. Simple Newtonian fluids did not adequately explain many difficulties in nature in the beginning. Numerous researchers have offered various non-Newtonian models that are not adequately covered by the straightforward Navier–Stokes theory in order to investigate these issues. Exact solutions to problems involving the free convection flow of viscous fluid are widely available in the literature. Because they are so common, non-Newtonian fluids are of interest to researchers. Researchers have proposed a number of mathematical models to comprehend the mechanics of non-Newtonian fluids since they have a wide variety of physical structures. These models are categorized as rate-type fluids or general differential form fluids. Maxwell<sup>1</sup> presents the Maxwell fluid idea.

Maxwell nanofluid flow across a porous rotating disk with the effect of heat transfer was studied by Ahmed et al.<sup>2</sup>. A Maxwell nanofluid's erratic flow while being heated by Newtonian radiation was examined by Raza and Asad<sup>3</sup>. The effects of heat transfer on the free convection flow of a hybrid Maxwell nanofluid down an indefinite vertical channel were examined by Ahmed et al.<sup>4</sup>. By combining the effects of an electric and magnetic field with the effects of thermal and changeable heat radiation, Khan et al.<sup>5</sup> research looked at the Maxwell nanofluid flow across a stretching surface. Maxwell nanofluid flow across a stretching porous medium with the influence of magnetohydrodynamics was discussed mathematically by Mukhtar et al.<sup>6</sup>. The mixed convection flow of the Maxwell nanofluid with the impact and ion slip of the hall was examined by Ibrahim and Abneesa<sup>7</sup>. The

<sup>1</sup>Department of Mathematics, City University of Science and Information Technology, Peshawar 25000, Khyber Pakhtunkhwa, Pakistan. <sup>2</sup>Basic Sciences Department, College of Science and Theoretical Studies, Saudi Electronic University, Abha Male 61421, Saudi Arabia. <sup>3</sup>Department of Mathematics, College of Science Al-Zulfi, Majmaah University, Al-Majmaah 11952, Saudi Arabia. <sup>4</sup>Center of Research, Faculty of Engineering, Future University in Egypt, New Cairo 11835, Egypt. ✉email: farhadali@cusit.edu.pk

Maxwell nanofluid flow across an infinite vertical with the influence of ramping and isothermal wall conditions was studied by Khan et al.<sup>8</sup>. The MHD Maxwell nanofluid flow across the porous stretched sheet with gyrotactic microorganisms is researched by Safdar et al.<sup>9</sup> and is discussed theoretically and numerically. The temperature and mass characteristics of the Soret-Dufour model of magnetized Maxwell nanofluid flow across a shrinking inclined plane were examined by Parvin et al.<sup>10</sup>. Ahmad et al.<sup>11</sup> examined the bio-convective Maxwell nanofluid flow via an exponentially stretched sheet with the convective boundary condition. Rasool et al.<sup>12</sup> examined the Darcy-Forchheimer medium and heat radiation in the magnetohydrodynamic (MHD) Maxwell nanofluid flow confronted to a stretched surface. Alsallami et al.<sup>13</sup> conducted a numerical analysis of the nanofluid flow across a heated rotating disc under the effects of Brownian motion, thermophoresis, and nonlinear radiation.

In a letter to Leibniz, L'Hospital posed an issue that led to the development of fractional calculus<sup>14</sup>. L'Hospital questioned anything about  $D^n f(r)/Dr^n$  this letter. When L'Hospital inquired about the result of  $n = 1/2$  Leibniz responded that it would initially seem to be a contradiction from which important insights would one day be drawn. Famous mathematicians including Euler, Laplace, Fourier, Lacroix, Abel, Riemann, and Liouville developed an interest in the subject after this conversation. They contributed to its growth. For a few decades, mathematicians were the only ones who had any knowledge of this topic. But in recent years, the idea of this topic has been expanded to various other disciplines in a number of different ways, including modeling speech signals<sup>15–20</sup>, modeling cardiac tissue electrode interface<sup>21</sup>, modeling sound wave propagation in solid permeable medium<sup>22</sup>, lateral and longitudinal governing of Sovran vehicle<sup>23</sup>, and so on. The most popular fractional derivatives were the Riemann–Liouville derivatives. These derivatives, however, had severe limitations and were only applicable to a specific class of issues. For instance, in the Riemann–Liouville fractional derivative, the constant does not result in zero when we take its derivative.

To address these shortcomings, Caputo develops a novel derivative, however the Caputo derivative's kernel remained singular. To address these concerns,<sup>24</sup> developed a new exponential function-based fractional operator without a solitary kernel in 2015. The Laplace transformation also works with the Caputo-Fabrizio (CF) derivative.<sup>25</sup> investigated the flow of a viscous fluid via an infinitely mobile plate. Due to its abstract nature, fractional calculus did not initially attract the attention of researchers. Its method has evolved over time from conceptual to practical, and as a result, it has gained popularity among scholars. Contrary to classical calculus, non-integer derivatives are much more prevalent in practically all scientific disciplines<sup>26–29</sup>.

The practical applications of local derivatives extend beyond engineering to include integrated circuits, electrochemistry, probability, curve fitting, and nuclear fusion<sup>30–32</sup>. Imran et al.<sup>33</sup> observed the rheology of fractional Maxwell fluid in the presence of Newtonian heating effects while keeping in mind the stated relevance. The authors changed a non-local model into a local mathematical fractional order model using the CF operator. In a Maxwell fluid with a CF derivative, Khan et al.<sup>34</sup> examined the evaluation of heat transfer over a fluctuating vertical plate. By generalizing it using the CF fractional derivative, Saqib et al.<sup>35</sup> explored the free convection flow of a hybrid nanofluid with heat transfer.

Nanofluids have a significant impact on a variety of industrial sectors where heat transmission is essential due to their enhanced thermal conductivity properties. In order to improve the thermal conductivity of ordinary fluids, Choi<sup>36</sup> created the contemporary theory of interruption of nanosized particles. Thermal insulation, energy production, nuclear reactor cooling, electricity processing, and cancer therapy are just a few of the many uses for nanofluids. Applications for nanofluids go beyond simply increasing the thermal conductivity of fluids; they also play a beneficial function in intelligent technology, drug delivery, disease diagnostics, food processing, and other areas<sup>37</sup>. The mechanical characteristics of nanoparticles were investigated by Guo et al.<sup>38</sup> for brand-new applications in a variety of industries, such as surface engineering, tribology, and coating.

Burg et al.<sup>39</sup> investigation of the fluid weights of individual cells, biomolecules, and nanoparticles was conducted. In a small shell-and-tube heat exchanger with and without a fin, Bahiraei and Monavari<sup>40</sup> investigated the impact of different nanoparticle morphologies on the thermal-hydraulic performance of a boehmite nanofluid.  $Al_2O_3$ -water nanofluid was used in Mazaheri et al.<sup>41</sup> investigation of the properties of a counter-flow four-layer microchannel heat exchanger. In their investigation of the pipe side, Bahiraei and Monavari<sup>42</sup> used water as the cold fluid and a nanofluid with five distinct particle morphologies as the hot fluid. In a triple-tube heat exchanger, a new crimped-spiral rib with irreversibility properties was used by Bahiraei et al.<sup>43</sup> in their study on thermal applications.

Oils are not always the greatest choice when it comes to lubricating parts. The lubricant may need to stick to a part in some situations. Regular maintenance is necessary to stop stains and damage caused by oil leaks, which is costly in terms of both time and money. Only the grease needs to be changed every 6 months, allowing one bearing to function until a roll change. More money has been saved by doing away with maintenance tasks like changing seal hearing. On the other hand, components that are difficult to obtain require lubrication. Grease-like semisolid lubricants, which share many characteristics with their fluid counterparts, are designed to stick to or adhere to the parts they are meant to lubricate. Grease is frequently used to lessen friction in machinery. Lubricating grease is made up of three ingredients: oil, thickener, and additives. The primary ingredients in grease formulations, base oil and additive kit, have a considerable impact on grease behavior. The thickening, which is also known as a sponge, keeps the lubricant in place. Grease can extend the life of equipment that is difficult to reach for multiple lubrications and worn sections that were previously lubricated with oil by keeping thicker films in wear-widened clearances. High-quality greases can lubricate uncommonly hard-to-reach components for extended periods of time without needing to be replenished on a regular basis. The centralized lubrication systems, electrical motors, bearings, truck wheel hubs for logging and mining equipment, construction, landscaping, and gearboxes are just a few of the sealed life applications that use these greases. In contemporary technologies including the oil business, sealing agents, the automotive industry, and the metalworking sector, grease has practical applications<sup>44–47</sup>. The tribological characteristics of conductive lubricating greases were explored by Fan et al.<sup>48</sup> who also covered experimental methods including scanning electron microscopy to study friction

processes. Grease qualities, especially those based on metal soap, depend not only on their composition but also on how the thickeners are prepared and mixed<sup>49</sup>.

From the above literature survey, it is evident that, no exact solutions are reported for Maxwell nanofluid flow using the CF fractional approach. To fill this gap, we have considered an open channel flow of Maxwell nanofluid together with heat and mass transfer. For this purpose, relevant constitutive equations have been used to model the problem in terms of classical PDEs and generalized using the Caputo-Fabrizio fractional derivative approach. The obtained fractional model is solved by jointly using two different mathematical tools, namely, the finite Fourier sine transform and the Laplace transform technique. More importantly, the current research focuses on using MoS<sub>2</sub> nanoparticles in grease to improve mechanical properties such as weak machine friction reduction, low heat transfer power, low lubrication, and various other mechanical problems.

### Mathematical formulation

In the present work, we assumed viscoelastic Maxwell nanofluid flow between two vertical parallel plates separated by a distance of  $d$ . The fluid motion is considered in  $x$  the direction in the presence of buoyancy force. To improve the rate of heat transfer, MoS<sub>2</sub> nanoparticles are suspended uniformly within the grease, which is taken as a base fluid. Initially, both the plate and fluid are at rest with ambient temperature  $T_{1\infty}$  and constant concentration  $C_{1\infty}$ . For  $t = 0^+$ , the temperature and concentration of the left plate increased to  $T_{1w}$  and  $C_{1w}$ . The governing equations of the given flow regime are as follows (Fig. 1):

In light of assumptions, the velocity, temperature and concentration fields are given as;

$$\vec{V} = (u(y, t)\hat{i}, 0\hat{j}, 0\hat{k}), \tag{1}$$

$$T = (T(y, t), 0, 0), \tag{2}$$

$$C = (C(y, t), 0, 0), \tag{3}$$

The continuity, momentum, heat and concentration equations in constitutive form are given as follow<sup>50,51</sup>:

$$\nabla \cdot \vec{V} = 0. \tag{4}$$

$$\rho \left[ \frac{\partial \vec{V}}{\partial t} \right] = \text{div} \mathbf{T} + \rho \vec{b} \tag{5}$$

$$\rho c_p \frac{\partial T}{\partial t} = k \nabla \times \nabla \times T, \tag{6}$$

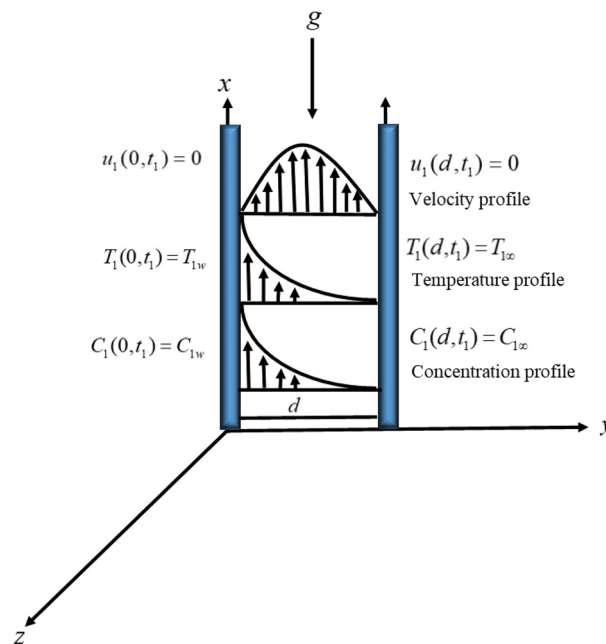


**Figure 1.** The physical configuration of the problem.

$$\frac{\partial C}{\partial t} = D\nabla \times \nabla \times C. \tag{7}$$

Keeping in view the assumption and Eqs. (1)–(3), Eqs. (5)–(7) will take the form:

$$\begin{aligned} \rho_{nf} \left( 1 + \lambda_1 \frac{\partial}{\partial t_1} \right) \frac{\partial u_1(y_1, t_1)}{\partial t_1} &= \mu_{nf} \frac{\partial^2 u_1(y_1, t_1)}{\partial y_1^2} + \left( 1 + \lambda_1 \frac{\partial}{\partial t_1} \right) (\rho\beta_T)_{nf} g (T_1(y_1, t_1) - T_{1\infty}) \\ &+ \left( 1 + \lambda_1 \frac{\partial}{\partial t_1} \right) (\rho\beta_C)_{nf} g (C_1 - C_{1\infty}), \end{aligned} \tag{8}$$

$$(\rho C_p)_{nf} \frac{\partial T_1}{\partial t_1} = k_{nf} \frac{\partial^2 T_1}{\partial y_1^2}, \tag{9}$$

$$\frac{\partial C_1}{\partial t_1} = D_{nf} \frac{\partial^2 C_1}{\partial y_1^2}. \tag{10}$$

Subject to the below imposed physical conditions:

$$\left. \begin{aligned} u_1(y_1, 0) = 0, \quad T_1(y_1, 0) = T_{1\infty}, \quad C_1(y_1, 0) = C_{1\infty}, \\ u_1(0, t) = 0, \quad T_1(0, t_1) = T_{1w}, \quad C(0, t_1) = C_{1w}, \\ u_1(\infty, t_1) = 0, \quad T_1(d, t_1) = T_{1\infty}, \quad C_1(d, t_1) = C_{1\infty}, \\ \left. \frac{\partial u_1(y_1, t_1)}{\partial t_1} \right|_{t_1=0} = 0 \end{aligned} \right\}. \tag{11}$$

In the above system of equations, the velocity component of the Maxwell nanofluid along the  $x$ -axis is denoted by  $u_1$ ,  $T_1$  is the fluid temperature,  $T_{1\infty}$  shows the ambient temperature, and  $T_{1w}$  is the wall temperature. The thermophysical properties of the grease and  $MoS_2$  nanoparticles are given in Table 1.

For nanofluids, expression of  $\rho_{nf}$ ,  $(\rho\beta)_{nf}$ ,  $(\rho c_p)_{nf}$ ,  $k_{nf}$ , is given by<sup>20</sup>.

$$\left. \begin{aligned} \rho_{nf} &= \rho_f(1 - \phi) + \phi\rho_s, \quad (\rho\beta_T)_{nf} = (\rho\beta_T)_f(1 - \phi) + \phi(\rho\beta_T)_s, \\ (\rho\beta_C)_{nf} &= \phi(\rho\beta_C)_s + (\rho\beta_C)_f(1 - \phi), \quad (\rho c_p)_{nf} = (1 - \phi)(\rho c_p)_f + \phi(\rho c_p)_s, \\ D_{nf} &= D_f(1 - \phi), \quad k_{nf} = k_f \left[ \frac{k_s + 2k_f - 2\phi(k_f - k_s)}{k_s + 2k_f + \phi(k_f - k_s)} \right], \quad \mu_{nf} = \mu_f(1 - \phi)^{-2.5}. \end{aligned} \right\}. \tag{12}$$

Nondimensional quantities are:

$$w = \frac{u_1}{U_0}, \quad \zeta = \frac{y_1}{d}, \quad \tau = \frac{t_1 U_0}{d}, \quad \theta = \frac{T_1 - T_{1\infty}}{T_{1w} - T_{1\infty}}, \quad \Phi = \frac{C_1 - C_{1\infty}}{C_{1w} - C_{1\infty}}. \tag{13}$$

Using Eq. (13), the dimensionless forms of Eqs. (8)–(11) are given as follows:

$$A_2 \left( 1 + \lambda \frac{\partial}{\partial \tau} \right) \frac{\partial w(\zeta, \tau)}{\partial \tau} = \frac{\partial^2 w(\zeta, \tau)}{\partial \zeta^2} + A \left( 1 + \lambda \frac{\partial}{\partial \tau} \right) Gr\Theta + A_1 \left( 1 + \lambda \frac{\partial}{\partial \tau} \right) Gm\Phi, \tag{14}$$

$$\frac{\partial \theta(\zeta, \tau)}{\partial \tau} = \frac{1}{\psi} \frac{\partial^2 \theta(\zeta, \tau)}{\partial \zeta^2}, \tag{15}$$

$$\frac{\partial \Phi(\zeta, \tau)}{\partial \tau} = \frac{1}{\varphi} \frac{\partial^2 \Phi(\zeta, \tau)}{\partial \zeta^2}. \tag{16}$$

Physical conditions in dimensionless form:

Material	$\rho$ (km <sup>-3</sup> )	$c_p$ (JKg <sup>-1</sup> K <sup>-1</sup> )	$k$ (wm <sup>-1</sup> K <sup>-1</sup> )	$\beta \times 10^{-5}$ (K <sup>-1</sup> )
Grease	883	2100	0.1450	0.00001616
MoS <sub>2</sub>	506×10 <sup>3</sup>	397.21	904.4	2.8424

**Table 1.** Thermophysical properties of grease and  $MoS_2$ <sup>44–49</sup>.

$$\left. \begin{aligned} w(w, 0) = 0, \quad \theta(w, 0) = 0, \quad \Phi(w, 0) = 0, \\ w(0, \tau) = 0, \quad \theta(0, \tau) = 1, \quad \Phi(0, \tau) = 1, \\ w(1, \tau) = 0, \quad \theta(1, \tau) = 0, \quad \Phi(1, \tau) = 0, \\ \left. \frac{\partial w(y, \tau)}{\partial t} \right|_{\tau=0} = 0. \end{aligned} \right\} \tag{17}$$

Were

$$\lambda = \frac{\lambda_1 U_0}{d}, \quad \ell = (1 - \phi) + \phi \frac{\rho_s}{\rho_f}, \quad \ell_1 = (1 - \phi) + \phi \frac{(\rho\beta_T)_s}{(\rho\beta_T)_f}, \quad \ell_2 = (1 - \phi) + \phi \frac{(\rho\beta_c)_s}{(\rho\beta_c)_f}, \quad \ell_3 = \frac{1}{(1 - \phi)^{2.5}},$$

$$Gr = \frac{g\beta_T \rho d^2 (T_w - T_d)}{U_0 \mu}, \quad Gm = \frac{g\beta_C \rho d^2 (C_w - C_d)}{U_0 \mu}, \quad Re = \frac{U_0 d}{\nu}, \quad A = Gr \ell_1 \ell_3, \quad A_1 = Gm \ell_2 \ell_3, \quad A_2 = \ell \ell_3 Re, \quad Pr = \frac{\mu C_p}{k},$$

$$\psi = \frac{Pr Re \phi_2}{\phi_1}, \quad Sc = \frac{\nu}{D_j}, \quad \varphi = \frac{Sc Re}{1 - \phi}.$$

**Exact solutions of the problem**

By applying the Caputo-Fabrizio (CF) time fractional derivative, Eqs. (14)–(16) will take the following shape:

$$A_2 (1 + \lambda^{CF} \wp_\tau^\alpha)^{CF} \wp_\tau^\alpha w(\zeta, \tau) = \frac{\partial^2 w(\zeta, \tau)}{\partial \zeta^2} + A (1 + \lambda^{CF} \wp_\tau^\alpha) Gr \theta(\zeta, \tau) + A_1 (1 + \lambda^{CF} \wp_\tau^\alpha) Gm \Phi(\zeta, \tau), \tag{18}$$

$${}^{CF} \wp_t^\alpha \theta(\zeta, \tau) = \frac{1}{\psi} \frac{\partial^2 \theta(\zeta, \tau)}{\partial \zeta^2}. \tag{19}$$

$${}^{CF} \wp_t^\alpha \Phi(\zeta, \tau) = \frac{1}{\varphi} \frac{\partial^2 \Phi(\zeta, \tau)}{\partial \zeta^2}, \tag{20}$$

where  ${}^{CF} D_t^\alpha (\cdot)$  is the CF time fractional operator, which is given by<sup>52</sup>:

$${}^{CF} D_t^\alpha f(t) = \frac{M(\alpha)}{(1 - \alpha)} \int_0^t \exp\left[-\frac{\alpha(t - \tau)}{1 - \alpha}\right] f'(\tau) d\tau. \tag{21}$$

where  $M(\alpha)$  is a normalization function such that  $M(0) = M(1) = 1$ .

**Solution of the energy equation.** By applying the Laplace transform technique to the Eq. (19) and incorporate IC's and BC's, we get:

$$\frac{d^2 \bar{\theta}}{d\zeta^2} = \frac{a \psi s \bar{\theta}(\zeta, s)}{s + a_1}, \tag{22}$$

By applying the finite Fourier sine transform to the Eq. (22), we get:

$$\bar{\Theta}_F(n, s) = \left( \frac{n\pi}{a_0 \psi + n\pi} \right) \left( \frac{a_1}{a_2 s} - \frac{a_1 - a_2}{a_2 (s + a_2)} \right), \tag{23}$$

By applying inverse Laplace transform on Eq. (23), we arrived at:

$$\Theta_F(n, \tau) = \frac{1 - (-1)^n}{n\pi} - \frac{(-1)^{n+1}}{n\pi} - a_3 \exp(-a_2 \tau), \tag{24}$$

where  $a_2 = \frac{a_1 (n\pi)^2}{a \psi + n\pi}$ ,  $a_3 = \left( \frac{n\pi}{a \psi + n\pi} \right) \left( \frac{a_1 - a_2}{a_2} \right)$ ,  $a = \frac{1}{1 - \alpha}$ ,  $a_1 = \frac{\alpha}{1 - \alpha}$

By applying inverse finite Fourier sine transform to Eq. (24), we get:

$$\theta(\zeta, \tau) = 1 - \zeta - 2 \sum_{n=1}^{\infty} a_3 \exp(-a\tau) \sin(n\pi \zeta). \tag{25}$$

**Solution of the concentration equation.** By applying the Laplace transform technique to Eq. (20) and incorporating ICs and BCs, we obtain:

$$\frac{d^2 \bar{\Phi}(\zeta, p)}{d\zeta^2} = \frac{a \varphi s \bar{\Phi}(\zeta, p)}{p + a_1}, \tag{26}$$

By applying the finite Fourier sine transform to Eq. (26), we obtain:

$$\bar{\Phi}_F(n, p) = \left( \frac{n\pi}{a\varphi - n\pi} \right) \left( \frac{a_1}{a_2 p} - \frac{a_1 - a_2}{a_2(p + a_2)} \right), \tag{27}$$

By applying the inverse Laplace transform to Eq. (27), we obtain:

$$\Phi_F(n, \tau) = \frac{1 - (-1)^n}{n\pi} - \frac{(-1)^{n+1}}{n\pi} - a_4 \exp(-a\tau), \tag{28}$$

Here,

$$a_4 = \frac{(a_1 - a_2)n\pi}{a_2(a\varphi - n\pi)}$$

By applying the inverse finite Fourier sine transform to Eq. (28), we obtain:

$$\Phi(\zeta, \tau) = 1 - \zeta - 2 \sum_{n=1}^{\infty} a_3 \exp(-a_2 t) \sin(n\pi \zeta). \tag{29}$$

**Solution of the momentum equation.** Applying the Laplace transform to Eq. (14) and incorporating ICs and BCs, we obtain:

$$\begin{aligned} \frac{ap\bar{w}(\zeta, p)(1 + \lambda p)A_2}{p + a} &= \frac{d^2\bar{w}}{d\zeta^2} + \left(1 + \frac{ap}{p + a}\right) \left(\frac{n\pi}{am + n\pi}\right) \left(\frac{p + a_1}{p(p + a_2)}\right) \\ &+ \left(1 + \frac{ap}{p + a}\right) \left(\frac{n\pi}{am_2 + n\pi}\right) \left(\frac{p + a_1}{p(p + a_2)}\right), \end{aligned} \tag{30}$$

By applying a sine finite Fourier transform to Eq. (30), we obtain

$$\begin{aligned} \bar{w}_F(n, p) &= \frac{1}{p} \left( \frac{a_1 A_{13} A_{18}}{a_2 A_{10} A_{11}} \right) + \frac{1}{p + a_2} \left( \frac{(a_1 A_{13} - a_1 a_2 - a_2 A_{13} - a_2^2) A_{18}}{a_2 (A_{10} - a_2) (-A_{11} + a_2)} \right) \\ &+ \frac{1}{p + A_{10}} \left( \frac{(a_1 A_{10} + A_{10}^2 - a_1 A_{13} + A_{10} A_{13}) A_{18}}{A_{10} (A_{10} - A_{11}) (A_{10} - a_2)} \right) \\ &+ \frac{1}{p + A_{11}} \left( \frac{(-a_1 A_{11} + A_{11}^2 + a_1 A_{13} - A_{11} A_{13}) A_{18}}{A_{11} (A_{10} - A_{11}) (A_{11} - a_2)} \right), \end{aligned} \tag{31}$$

By applying the inverse Laplace transform to Eq. (31), we obtain the following form:

$$\begin{aligned} w_F(n, \tau) &= \frac{a_1 A_{13} A_{18}}{a_2 A_{10} A_{11}} + \left( \frac{(a_1 A_{13} - a_1 a_2 - a_2 A_{13} - a_2^2) A_{18}}{a_2 (A_{10} - a_2) (-A_{11} + a_2)} \right) e^{-a_2 \tau} \\ &+ \left( \frac{(a_1 A_{10} + A_{10}^2 - a_1 A_{13} + A_{10} A_{13}) A_{18}}{A_{10} (A_{10} - A_{11}) (A_{10} - a_2)} \right) e^{-A_{10} \tau} \\ &+ \left( \frac{(-a_1 A_{11} + A_{11}^2 + a_1 A_{13} - A_{11} A_{13}) A_{18}}{A_{11} (A_{10} - A_{11}) (A_{11} - a_2)} \right) e^{-A_{10} \tau}, \end{aligned} \tag{32}$$

Now, apply the inverse finite Fourier sine transform to Eq. (32) to obtain the following form:

$$w(\zeta, \tau) = 2 \sum_{n=1}^{\infty} \left( \frac{a_1 A_{13} A_{18}}{a_2 A_{10} A_{11}} + \left( \frac{(a_1 A_{13} - a_1 a_2 - a_2 A_{13} - a_2^2) A_{18}}{a_2 (A_{10} - a_2) (-A_{11} + a_2)} \right) e^{-a_2 \tau} + \left( \frac{(a_1 A_{10} + A_{10}^2 - a_1 A_{13} + A_{10} A_{13}) A_{18}}{A_{10} (A_{10} - A_{11}) (A_{10} - a_2)} \right) e^{-A_{10} \tau} + \left( \frac{(-a_1 A_{11} + A_{11}^2 + a_1 A_{13} - A_{11} A_{13}) A_{18}}{A_{11} (A_{10} - A_{11}) (A_{11} - a_2)} \right) e^{-A_{10} \tau} \right) \sin(n\pi \zeta). \tag{33}$$

Introduced some constant

$$A_5 = aA_2, A_6 = \lambda A_5, A_7 = A_5 + (n\pi)^2, A_8 = a_1(n\pi)^2, A_9 = \sqrt{\frac{A_7 - 4A_8}{2}},$$

$$A_{10} = \frac{A_7}{2} + A_9, A_{11} = \frac{A_7}{2} - A_9, A_{12} = a + 1, A_{13} = \frac{a_1}{A_{12}}, A_{14} = A_{12}A, A_{15} = A_{12}A_1,$$

$$A_{16} = \frac{A_{14}(n\pi)}{am + n\pi}, A_{17} = \frac{A_{15}(n\pi)}{am_2 + n\pi}, A_{18} = A_{16} + A_{17}.$$

**Nusselt number.** The dimensional form of the Nusselt number for a Maxwell nanofluid is given by<sup>8</sup>:

$$Nu = -\frac{k_{nf}}{k_f} \left( \frac{d}{T_{1w} - T_{1\infty}} \right) \frac{\partial T_1}{\partial y_1} \Big|_{y_1=0} \quad (34)$$

By using Eq. (13), the dimensionless form of Eq. (34) becomes:

$$Nu = -\frac{k_{nf}}{k_f} \frac{\partial \theta}{\partial \zeta} \Big|_{\zeta=0} \quad (35)$$

**Sherwood number.** The dimensional form of the Sherwood number for a Maxwell nanofluid is given by<sup>8</sup>:

$$Sh = -D_{nf} \left( \frac{d}{C_{1w} - C_{1\infty}} \right) \frac{\partial C_1}{\partial y_1} \Big|_{y_1=0} \quad (36)$$

By using Eq. (13), the dimensionless form of Eq. (36) becomes:

$$Sh = -D_{nf} \frac{\partial \Phi}{\partial \zeta} \Big|_{\zeta=0} \quad (37)$$

**Skin friction.** The dimensional form of nonzero shear stress for Maxwell fluid is given as:

$$\tau_{xy}^* = \frac{\mu_f}{(1 + \lambda \frac{\partial}{\partial \tau})} \frac{\partial u_1}{\partial y_1}, \quad (38)$$

For a Maxwell nanofluid, Eq. (38) takes the following form:

$$\tau_{xy}^* = \frac{\mu_{nf}}{(1 + \lambda \frac{\partial}{\partial \tau})} \frac{\partial u_1}{\partial y_1}, \quad (39)$$

By using Eq. (12) and Eq. (13), the dimensionless form of Eq. (39) becomes:

$$Sf_{lp} = \frac{1}{(1 - \phi)^{2.5}} \frac{1}{(1 + \lambda \frac{\partial}{\partial \tau})} \frac{\partial w}{\partial \zeta}, \quad (40)$$

where  $\tau_{xy}^* = \frac{\tau_{xy}^* d}{\mu_f U_0}$  is the dimensionless form of nonzero shear stress and  $\lambda = \frac{\lambda_1 U_0}{d}$  is the dimensionless Maxwell parameter.

This problem is considered for the flow of Maxwell nanofluids through vertical plates. Therefore, the skin friction on the left and right plates is given by:

$$Sf_{lp} = \frac{1}{(1 - \phi)^{2.5}} \frac{1}{(1 + \lambda \frac{\partial}{\partial \tau})} \frac{\partial w}{\partial \zeta} \Big|_{\zeta=0} \quad (41)$$

$$Sf_{rp} = \frac{1}{(1 - \phi)^{2.5}} \frac{1}{(1 + \lambda \frac{\partial}{\partial \tau})} \frac{\partial w}{\partial \zeta} \Big|_{\zeta=1} \quad (42)$$

where  $Sf_{lp}$  and  $Sf_{rp}$  denote the skin friction at the left and right plates, respectively.

### Special case

The obtained results given in Eqs. (25), (29) and (33) can be reduced to the results published by Khalid et al.<sup>53</sup> by ignoring  $\lambda \rightarrow 0$ ,  $\alpha \rightarrow 1$  and mass Grashof number  $Gm$ .

### Results and discussion

This section includes the definitive explanation of the Maxwell fluid model free convection flow. Approaching nondimensional variables is applied to make the PDE system dimensionless. The fractional Maxwell fluid model has been developed by implementing the CF time-fractional derivative. The joint use of the Laplace and

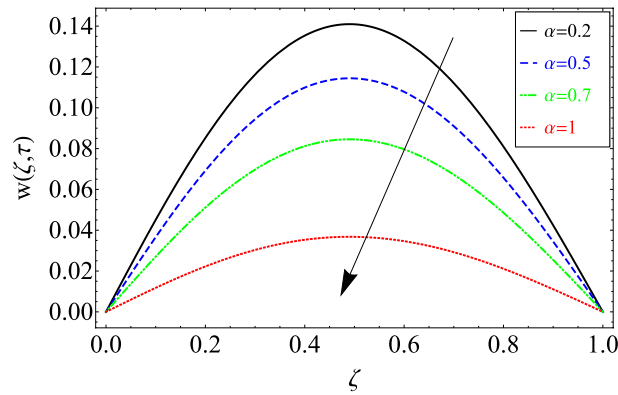


**Figure 2.** The effect of different values of  $\alpha$  on velocity distribution of Maxwell nanofluid, when  $Re = 10$ ,  $\tau = 0.5$ ,  $\phi = 0.02$ ,  $Gr = 0.05$ ,  $Gm = 0.5$ ,  $Pr = 6300$ ,  $Sc = 15$  and  $\lambda = 0.5$ .

Sine Finite Fourier techniques evaluated exact results for velocity, temperature, and concentration profiles. The thermophysical properties of  $MoS_2$  nanoparticles and grease are given in Table 1. The graphical analysis shows various embedded parameters  $\alpha$ ,  $\tau$ ,  $\lambda$ ,  $Gm$ ,  $Gr$ ,  $Re$ ,  $Sc$  and  $\phi$  on velocity, temperature, and concentration profiles. Furthermore, in Figs. 2, 3, 4, 5, 6, 7 and 8, the impact of sundry parameters on the velocity distribution is shown. The impact of sundry parameters on the temperature profile is shown graphically in Figs. 9 and 10. Finally, the impact of embedded parameters on the concentration distribution is shown graphically in Figs. 11 and 12.

Figure 2 is plotted to analyze flow rheology in response to fractional parameters  $\alpha$ . The prime benefit of the fractional model is that it provides more than one fluid layer for the investigation of fluid behavior. It gives the

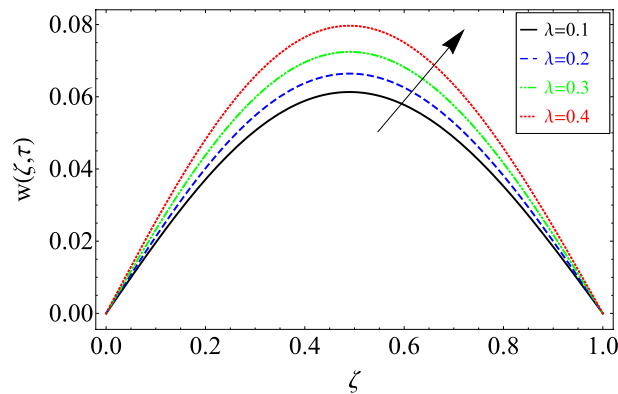


**Figure 3.** The effect of different values of  $\lambda$  on velocity distribution of Maxwell nanofluid, when  $Re = 10$ ,  $\alpha = 0.7$ ,  $\tau = 0.5$ ,  $\phi = 0.02$ ,  $Gr = 0.05$ ,  $Pr = 6300$ ,  $Sc = 15$  and  $Gm = 0.5$ .

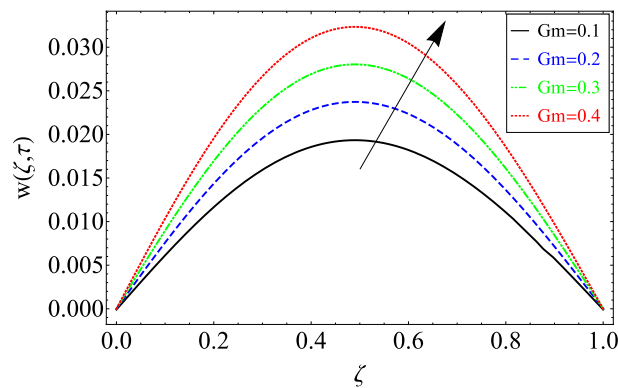


**Figure 4.** The effect of different values of  $Gm$  on velocity distribution of Maxwell nanofluid, when  $Re = 10$ ,  $\alpha = 0.7$ ,  $\tau = 0.5$ ,  $\phi = 0.02$ ,  $Gr = 0.05$ ,  $Pr = 6300$ ,  $Sc = 15$  and  $\lambda = 0.5$ .



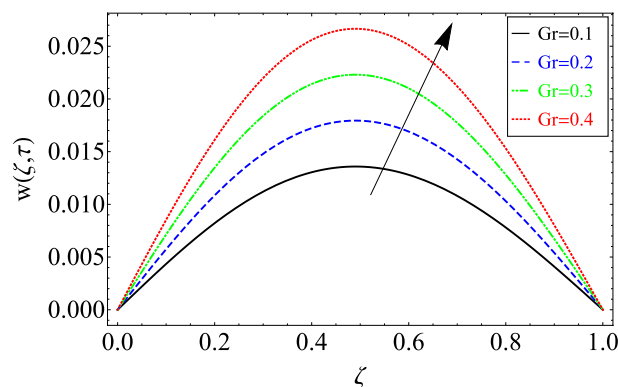


**Figure 5.** The effect of different values of  $Gr$  on velocity distribution of Maxwell nanofluid, when  $Re = 10$ ,  $\alpha = 0.7$ ,  $\tau = 0.5$ ,  $\phi = 0.02$ ,  $Gm = 0.5$ ,  $Pr = 6300$ ,  $Sc = 15$  and  $\lambda = 0.5$ .

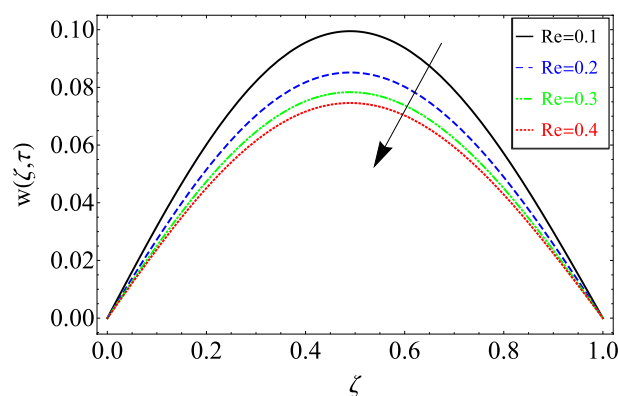


**Figure 6.** The effect of different values of  $Re$  on velocity distribution of Maxwell nanofluid, when  $\alpha = 0.7$ ,  $\tau = 0.5$ ,  $\phi = 0.02$ ,  $Gm = 0.5$ ,  $Gr = 0.05$ ,  $Pr = 6300$ ,  $Sc = 15$  and  $\lambda = 0.5$ .

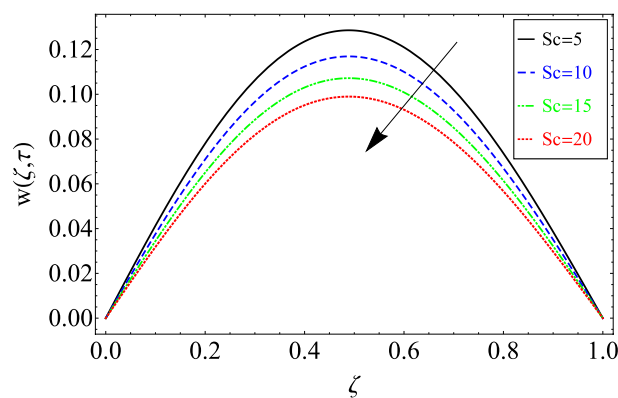


**Figure 7.** The effect of different values of  $Sc$  on velocity distribution of Maxwell nanofluid, when  $\alpha = 0.7$ ,  $\tau = 0.5$ ,  $\phi = 0.02$ ,  $Gm = 0.5$ ,  $Gr = 0.05$ ,  $Pr = 6300$ ,  $Re = 10$  and  $\lambda = 0.5$ .

experimentalist and researchers more options for comparing their research to the fractional model, which is impossible by a classical mathematical model.

The velocity of the Maxwell nanofluid against the material parameter  $\lambda$  is portrayed in Fig. 3. It can be seen from the expression of the material parameter that directly relates to the fluid's viscosity. Therefore, by raising the values of  $\lambda$ , the viscous forces increase, which leads to a decrease in fluid motion.

The impact of mass Grashof number  $Gm$  on the velocity field has been plotted in Fig. 4. From the figure it can be seen clearly that velocity profile enhances for greater magnitude of  $Gm$ . This trend in the velocity field is physically true because when the value of  $Gm$  increases the concentration level near the plate increase and we

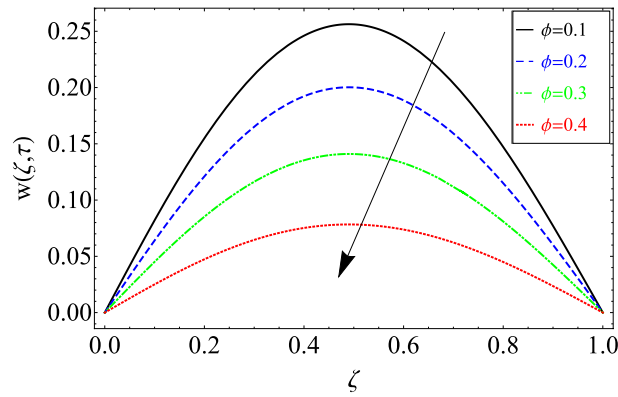


**Figure 8.** The effect of different value of  $\phi$  on velocity distribution of Maxwell nanofluid, when  $\alpha = 0.7$ ,  $\tau = 0.5$ ,  $Sc = 15$ ,  $Gm = 0.5$ ,  $Gr = 0.05$ ,  $Pr = 6300$ ,  $Re = 10$  and  $\lambda = 0.5$ .

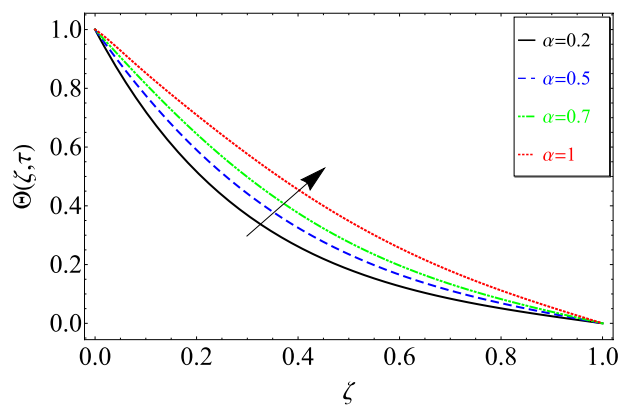


**Figure 9.** The effect of different values of  $\alpha$  on temperature distribution of Maxwell nanofluid, when  $\phi = 0.02$  and  $Pr = 6300$ .

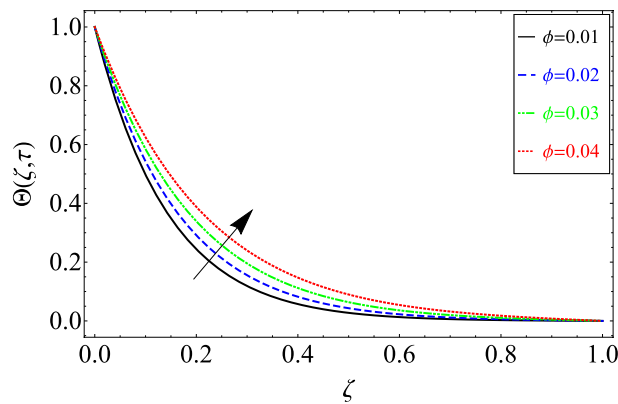


**Figure 10.** The effect of different values of  $\phi$  on Temperature distribution of Maxwell nanofluid, when  $\alpha = 0.7$  and  $Pr = 6300$ .

know that fluid moves from higher concentration area to lower concentration area, therefore increasing trend has been observed.

The up shots of  $Gr$  on the velocity field of grease have been plotted in Fig. 5. Increasing behavior has also been noticed for the increasing values of  $Gr$ . Physically, this trend is true because the greater magnitude of  $Gr$  weakens the boundary layer of the fluid and produces bouncy forces in the fluid. Due to these effects, the fluid motion accelerates.

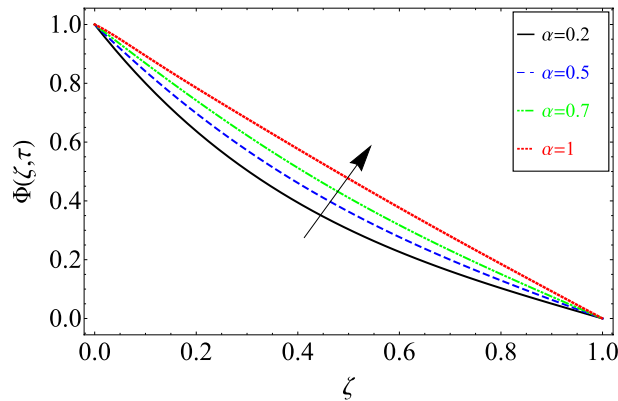


**Figure 11.** The effect of different values of  $\alpha$  on concentration distribution of Maxwell nanofluid, when  $\phi = 0.02$  and  $Sc = 20$ .

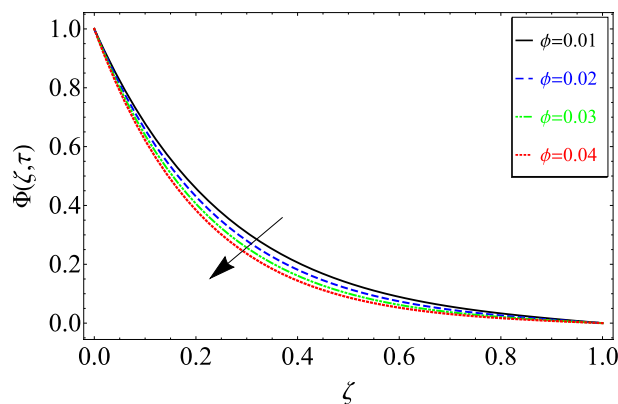


**Figure 12.** The effect of different values of  $\phi$  on concentration distribution of Maxwell nanofluid, when  $\alpha = 0.7$  and  $Sc = 20$ .

The effect of Reynolds number  $Re$  on velocity profile has been portrayed in Fig. 6. It can be seen from the figure that velocity profile shows decreasing trend for greater magnitude of  $Re$ . Physically,  $Re$  shows the relation between inertial forces and viscous forces. As the value of  $Re$  increase the viscous forces in the fluid enhance as a result the momentum boundary become thick and slow down the fluid.

Figure 7 shows  $Sc$  influence on the nanofluid velocity of Maxwell. The Maxwell nanofluid velocity is investigated by increasing  $Sc$ . Since  $Sc$  is the ratio of mass diffusion to viscous forces, raising  $Sc$  increases viscous forces and reduces mass diffusion, which reduces velocity.

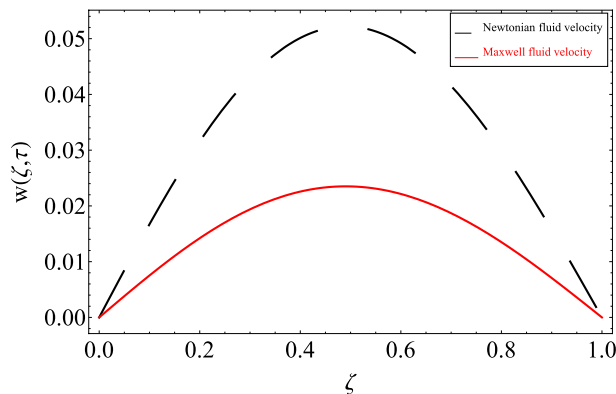
Figure 8 depicts the variance in the velocity profile over a variety of different values of  $\phi$ . This figure shows that increasing the values of  $\phi$  decreases its velocity. The reason for the decrease in velocity is that when  $\phi$  rises, the fluid viscosity increases, resulting in the retardation of velocity.

Figure 9 displays the impact of fractional parameter  $\alpha$  on temperature. This figure also shows the behavior of the temperature distribution for classical order by taking  $\alpha = 1$  as well as fractional order  $0 < \alpha < 1$  compared to classical models. The fractional model is more generalized, more effective for describing the memory effect, and provides a wide range of solutions. Compared to the classical Maxwell nanofluid model, the fractional-order Maxwell nanofluid model provides a better explanation of heat transfer by varying degrees.

Figure 10 shows the effect of  $\phi$  on the temperature distribution. An increase in the temperature distribution is noticed for increasing values of  $\phi$ . Regular grease has low thermal conductivity and lubrication properties.  $MoS_2$  has a high thermal conductivity, which will increase the heat transfer rate of regular grease and the thermal conductivity of regular grease. As  $MoS_2$  is also used as a dry lubricant, it will also increase the lubricity of regular grease.

Figure 11 shows the time fractional order parameter impacts on the concentration distribution. This figure shows the behavior of the concentration distribution for classical order  $\alpha = 1$  and fractional order  $0 < \alpha < 1$ . The same trend has been noticed in response to the fractional order parameter, as we discussed in Fig. 9.

Figure 12 shows the impact of  $\phi$  on the concentration distribution. As seen in the figure, the concentration distribution decreases with increasing values of  $\phi$ . The reason for this phenomenon is that when the concentration distribution decreases, viscous forces rise.



**Figure 13.** Comparison of the present results with the published results of Khalid et al.<sup>53</sup>.

$\lambda$	$Gm$	$Gr$	$Pr$	$Re$	$\alpha$	$\tau$	$\phi$	$Sc$	$C_f^\alpha$	$C_f^{classical}$
0.2	1.5	1.5	6000	0.7	0.6	1.7	0.02	10		
0.3	1.5	1.5	6000	0.7	0.6	1.7	0.02	10	8.598	25.549
0.2	2.5	1.5	6000	0.7	0.6	1.7	0.02	10	9.581	15.622
0.2	1.5	2.5	6000	0.7	0.6	1.7	0.02	10	28.659	50.764
0.2	1.5	1.5	6500	0.7	0.6	1.7	0.02	10	6.461	20.192
0.2	1.5	1.5	6000	0.8	0.6	1.7	0.02	10	9.206	23.556
0.2	1.5	1.5	6000	0.7	0.7	1.7	0.02	10	14.039	21.746
0.2	1.5	1.5	6000	0.7	0.6	1.8	0.02	10	10.132	25.336
0.2	1.5	1.5	6000	0.7	0.6	1.7	0.04	10	13.713	34.406
0.2	1.5	1.5	6000	0.7	0.6	1.7	0.02	15	8.234	22.476

**Table 2.** Skin friction of grease based  $MoS_2$  Maxwell nanofluid on the left plate.

$\lambda$	$Gm$	$Gr$	$Pr$	$Re$	$\alpha$	$\tau$	$\phi$	$Sc$	$C_f^\alpha$	$C_f^{classical}$
0.2	1.5	1.5	6000	0.7	0.6	1.7	0.02	10		
0.3	1.5	1.5	6000	0.7	0.6	1.7	0.02	10	7.598	28.549
0.2	2.5	1.5	6000	0.7	0.6	1.7	0.02	10	12.581	18.622
0.2	1.5	2.5	6000	0.7	0.6	1.7	0.02	10	18.659	55.764
0.2	1.5	1.5	6500	0.7	0.6	1.7	0.02	10	27.461	22.192
0.2	1.5	1.5	6000	0.8	0.6	1.7	0.02	10	6.206	13.556
0.2	1.5	1.5	6000	0.7	0.7	1.7	0.02	10	15.039	21.746
0.2	1.5	1.5	6000	0.7	0.6	1.8	0.02	10	13.132	25.336
0.2	1.5	1.5	6000	0.7	0.6	1.7	0.04	10	15.713	7.406
0.2	1.5	1.5	6000	0.7	0.6	1.7	0.02	15	9.234	26.476

**Table 3.** Skin friction of grease based  $MoS_2$  Maxwell nanofluid on the right plate.

Figure 13 compares our findings to the findings of the published article of Khalid, et al.<sup>53</sup> to validate our obtained solutions. From this figure, our results matched the results of Khalid et al.<sup>53</sup> by taking  $\lambda \rightarrow 0$ ,  $\alpha \rightarrow 1$  and  $Gm \rightarrow 0$ .

The variation in skin friction on the lower and upper plates is shown in Tables 2 and 3. These tables display the effects of skin friction for fractional and classical Maxwell nanofluid models along with other physical parameters. Tables 4 and 5 depict the Nusselt and Sherwood number variations, respectively, for distinct values of  $\phi$ . The heat transfer rate increases to 12.38%, and the mass distribution decreases to 2.14% by adding nanoparticles up to 4%.

$\phi$	$Nu$	Heat transfer enhancement
0.00	162.42	
0.01	169.783	4.3098%
0.02	177.406	9.2266%
0.03	185.296	14.0844%
0.04	193.466	19.1146%

**Table 4.** Variation in the rate of mass transfer grease-based  $MoS_2$ .

$\phi$	$Sh$	Decrease in mass distribution
0.00	0.6926	
0.01	0.6967	0.5919%
0.02	0.7010	1.2128%
0.03	0.7054	1.8481%
0.04	0.7100	2.5122%

**Table 5.** Variation in the rate of mass transfer grease-based  $MoS_2$ .

### Concluding remarks

The goal of this study is to examine closed-form solutions for Maxwell nanofluid flow in open channels.  $MoS_2$  nanoparticles are used, while grease is the basis fluid. The Caputo-Fabrizio fractional derivative, which has lately emerged as the most popular fractional derivative, is then used to generalize the classical model. Through the use of the finite Fourier, sine transform and the Laplace transform technique, the coupled system's solutions are achieved. The collected results are also depicted in the graphs. The study's primary outcomes are listed below.

- The variations in all the profiles are shown for different values of  $\alpha$ . It is important here to mention that we have different lines for one value of time. This effect is showing the memory effect in the fluid, which cannot be demonstrated from the integer order derivative.
- The present results are reducible to the classical Maxwell nanofluid model by taking  $\alpha \rightarrow 1$ .
- The velocity of Maxwell nanofluid decrease by increasing the amount of  $MoS_2$  nanoparticles.
- Using nanoparticles in the grease increases the heat transfer rate which will off course increase life time, friction and lubrication in different engines and machinery.
- The Maxwell nanofluid velocity profile increases with respect to  $\lambda$ ,  $Gm$ , and  $Gr$ .
- By rising the value of  $\phi$  enhanced heat transfers up to 11.46%.
- The rate of mass transfer decreases to 2.5122% of regular grease.

### Future suggestions

Here are some recommendations for extending the aforementioned challenge for forthcoming researchers.

- Cylindrical co-ordinates can be added to the scope of this issue.
- Various nanoparticles can be added for a variety of purposes.
- The proposed method can be used to represent a variety of non-Newtonian fluids, including second-grade fluid, Jeffery fluid, Couple stress fluid, and others.

### Data availability

The datasets used and analyzed during the current study available from the corresponding author on reasonable request.

Received: 30 December 2021; Accepted: 14 March 2023

Published online: 17 March 2023

### References

1. Maxwell, J. C. (1831–1879) A treatise on electricity and magnetism. Vol. 1. In *Lilliad - Univ. Lille—Sci. Technol.* (1873) (accessed 22 Sep 2021); <https://iris.univ-lille.fr/handle/1908/3097>.
2. Ahmed, J., Khan, M. & Ahmad, L. Stagnation point flow of Maxwell nanofluid over a permeable rotating disk with heat source/sink. *J. Mol. Liq.* **287**, 110853. <https://doi.org/10.1016/j.MOLLIQ.2019.04.130> (2019).
3. Raza, N. & Ullah, M. A. A comparative study of heat transfer analysis of fractional Maxwell fluid by using Caputo and Caputo-Fabrizio derivatives. *Can. J. Phys.* **98**(1), 89–101. <https://doi.org/10.1139/CJP-2018-0602> (2019).
4. Ahmad, M., Imran, M. A. & Nazar, M. Mathematical modeling of (Cu–Al<sub>2</sub>O<sub>3</sub>) water based Maxwell hybrid nanofluids with Caputo-Fabrizio fractional derivative. *Adv. Mech. Eng.* **12**(9), 1–11. <https://doi.org/10.1177/1687814020958841> (2014).

5. Khan, H. *et al.* The combined magneto hydrodynamic and electric field effect on an unsteady maxwell nanofluid flow over a stretching surface under the influence of variable heat and thermal radiation. *Appl. Sci.* **8**(2), 160. <https://doi.org/10.3390/APP802160> (2018).
6. Mukhtar, T., Jamshed, W., Aziz, A. & Al-Kouz, W. Computational investigation of heat transfer in a flow subjected to magneto-hydrodynamic of Maxwell nanofluid over a stretched flat sheet with thermal radiation. *Numer. Methods Part. Differ. Equ.* <https://doi.org/10.1002/NUM.22643> (2020).
7. Ibrahim, W. & Anbessa, T. Mixed convection flow of a Maxwell nanofluid with Hall and ion-slip impacts employing the spectral relaxation method. *Heat Transf.* **49**(5), 3094–3118. <https://doi.org/10.1002/HTJ.21764> (2020).
8. Khan, N. *et al.* Maxwell nanofluid flow over an infinite vertical plate with ramped and isothermal wall temperature and concentration. *Math. Probl. Eng.* <https://doi.org/10.1155/2021/3536773> (2021).
9. Safdar, R. *et al.* Thermal radiative mixed convection flow of MHD Maxwell nanofluid: Implementation of buongiorno's model. *Chin. J. Phys.* **77**, 1465–1478. <https://doi.org/10.1016/J.CJPH.2021.11.022> (2022).
10. Parvin, S. *et al.* The flow, thermal and mass properties of Soret-Dufour model of magnetized Maxwell nanofluid flow over a shrinkage inclined surface. *PLoS ONE* **17**(4), e0267148. <https://doi.org/10.1371/JOURNAL.PONE.0267148> (2022).
11. Ahmad, S., Naveed-Khan, M. & Nadeem, S. Unsteady three dimensional bioconvective flow of Maxwell nanofluid over an exponentially stretching sheet with variable thermal conductivity and chemical reaction. *Int. J. Ambient Energy* <https://doi.org/10.1080/01430750.2022.2029765> (2022).
12. Rasool, G. *et al.* Significance of Rosselands Radiative process on reactive Maxwell nanofluid flows over an isothermally heated stretching sheet in the presence of Darcy-Forchheimer and Lorentz forces: Towards a new perspective on Buongiorno's model. *Micromachines* **13**(3), 368. <https://doi.org/10.3390/M113030368> (2022).
13. Alsallami, S. A. M. *et al.* "Numerical simulation of Marangoni Maxwell nanofluid flow with Arrhenius activation energy and entropy anatomization over a rotating disk. *Waves Random Compl. Med.* <https://doi.org/10.1080/17455030.2022.2045385> (2022).
14. Leibniz, G. W. Letter from Hanover; Germany; to G.F.A. L'Hopital. *Math. Schriften* **2**, 301–302 (2022).
15. Shah, J. *et al.* MHD flow of time-fractional Casson nanofluid using generalized Fourier and Fick's laws over an inclined channel with applications of gold nanoparticles. *Sci. Rep.* **12**, 1. <https://doi.org/10.1038/s41598-022-21006-9> (2022).
16. Sebaa, N., Fellah, Z. E. A., Lauriks, W. & Depollier, C. Application of fractional calculus to ultrasonic wave propagation in human cancellous bone. *Signal Process.* **86**(10), 2668–2677. <https://doi.org/10.1016/j.sigpro.2006.02.015> (2006).
17. Ahmad, Z. *et al.* Dynamics of love affair of Romeo and Juliet through modern mathematical tools: A critical analysis via fractal-fractional differential operator. *Fractals* **30**(05), 1–13. <https://doi.org/10.1142/S0218348X22401673> (2022).
18. Murtaza, S., Kumam, P., Kaewkhao, A., Khan, N. & Ahmad, Z. Fractal fractional analysis of non linear electro osmotic flow with cadmium telluride nanoparticles. *Sci. Rep.* **12**(1), 1–16. <https://doi.org/10.1038/s41598-022-23182-0> (2022).
19. Ahmad, Z., Ali, F., Khan, N. & Khan, I. Dynamics of fractal-fractional model of a new chaotic system of integrated circuit with Mittag-Leffler kernel. *Chaos Solit. Fract.* **153**, 111602. <https://doi.org/10.1016/J.CHAOS.2021.111602> (2021).
20. Khan, N. *et al.* Dynamics of chaotic system based on image encryption through fractal-fractional operator of non-local kernel. *AIP Adv.* **12**(5), 055129. <https://doi.org/10.1063/5.0085960> (2022).
21. Magin, R. L. & Ovadia, M. Modeling the cardiac tissue electrode interface using fractional calculus. *J. Vib. Control* **14**(9–10), 1431–1442. <https://doi.org/10.1177/1077546307087439> (2008).
22. Fellah, Z. E. A., Depollier, C. & Fellah, M. Application of fractional calculus to the sound waves propagation in rigid porous materials: Validation via ultrasonic measurements. *Acta Acust. Unit. Acust.* **88**(1), 34–39 (2002).
23. Suárez, J. I., Vinagre, B. M., Calderón, A. J., Monje, C. A. & Chen, Y. Q. Using fractional calculus for lateral and longitudinal control of autonomous vehicles. *Lect. Notes Comput. Sci.* **2809**, 337–348. [https://doi.org/10.1007/978-3-540-45210-2\\_31](https://doi.org/10.1007/978-3-540-45210-2_31) (2003).
24. Caputo, M. & Fabrizio, M. A new definition of fractional derivative without singular kernel. *Prog. Fract. Differ. Appl.* **1**(2), 73–85. <https://doi.org/10.12785/PFDA/010201> (2015).
25. Zafar, A. A. & Fetecau, C. Flow over an infinite plate of a viscous fluid with non-integer order derivative without singular kernel. *Alexandr. Eng. J.* **55**(3), 2789–2796. <https://doi.org/10.1016/j.aej.2016.07.022> (2016).
26. Ali, F. *et al.* A report of generalized blood flow model with heat conduction between blood and particles computational mathematics group project view project reliable numerical techniques for the solution of epidemic models with non-homogeneous population view project a report of generalized blood flow model with heat conduction between blood and particles. *Artic. J. Magn.* **27**(2), 186–200. <https://doi.org/10.4283/JMAG.2022.27.2.186> (2022).
27. Ali, F., Haq, F., Khan, N., Imtiaz, A. & Khan, I. A time fractional model of hemodynamic two-phase flow with heat conduction between blood and particles: Applications in health science. *Waves Random Compl. Media* **2022**, 1–28. <https://doi.org/10.1080/17455030.2022.2100002> (2022).
28. Ahmad, Z., Arif, M. & Khan, I. Dynamics of fractional order SIR model with a case study of COVID-19 in Turkey. *City Univ. Int. J. Comput. Anal.* **4**(01), 18–35. <https://doi.org/10.33959/CUIJCA.V4I01.43> (2020).
29. Murtaza, S., Ali, F., Aamina, N. A., Sheikh, I. K. & Nisar, K. S. Exact analysis of non-linear fractionalized jeffrey fluid. A novel approach of Atangana-Baleanu fractional Model. *Comput. Mater. Contin.* **65**(3), 2033–2047. <https://doi.org/10.32604/CMC.2020.011817> (2020).
30. Murtaza, S., Iftekhar, M., Ali-Aamina, F. & Khan, I. Exact Analysis of non-linear electro-osmotic flow of generalized maxwell nanofluid: Applications in concrete based nano-materials. *IEEE Access* **8**, 96738–96747. <https://doi.org/10.1109/ACCESS.2020.2988259> (2020).
31. Hasin, F., Ahmad, Z., Ali, F., Khan, N. & Khan, I. A time fractional model of Brinkman-type nanofluid with ramped wall temperature and concentration. *Adv. Mech. Eng.* **14**(5), 168781322210960. <https://doi.org/10.1177/16878132221096012> (2022).
32. Ahmad, Z., Ali, F., Alqahtani, A. M., Khan, N. & Khan, I. Dynamics of cooperative reactions based on chemical kinetics with reaction speed: A comparative analysis with singular and nonsingular kernels. *Fractals* **30**, 1. <https://doi.org/10.1142/S0218348X22400485> (2021).
33. Imran, M. A., Riaz, M. B., Shah, N. A. & Zafar, A. A. Boundary layer flow of MHD generalized Maxwell fluid over an exponentially accelerated infinite vertical surface with slip and Newtonian heating at the boundary. *Results Phys.* **8**, 1061–1067. <https://doi.org/10.1016/J.RINP.2018.01.036> (2018).
34. Khan, I., Ali-Shah, N., Mahsud, Y. & Vieru, D. Heat transfer analysis in a Maxwell fluid over an oscillating vertical plate using fractional Caputo-Fabrizio derivatives. *Eur. Phys. J. Plus* **132**(4), 1–12. <https://doi.org/10.1140/EPJP/I2017-11456-2> (2017).
35. Saqib, M., Khan, I. & Shafie, S. Application of fractional differential equations to heat transfer in hybrid nanofluid: modeling and solution via integral transforms. *Adv. Differ. Equ.* **2019**(1), 1–18. <https://doi.org/10.1186/S13662-019-1988-5> (2019).
36. Choi, S. & Eastman, J. Enhancing thermal conductivity of fluids with nanoparticles, 1995, (accessed 20 Sep 2021); <https://www.osti.gov/biblio/196525>.
37. Ali, F., Murtaza, S., Sheikh, N. A. & Khan, I. Heat transfer analysis of generalized Jeffery nanofluid in a rotating frame: Atangana-Baleanu and Caputo-Fabrizio fractional models. *Chaos Solitons Fract.* **129**, 1–15. <https://doi.org/10.1016/J.CHAOS.2019.08.013> (2019).
38. Guo, D., Xie, G. & Luo, J. Mechanical properties of nanoparticles: basics and applications. *J. Phys. D: Appl. Phys.* **47**(1), 013001. <https://doi.org/10.1088/0022-3727/47/1/013001> (2013).
39. Burg, T. P. *et al.* Weighing of biomolecules, single cells and single nanoparticles in fluid. *Nature* **446**(7139), 1066–1069. <https://doi.org/10.1038/nature05741> (2007).

40. Bahiraei, M. & Monavari, A. Thermohydraulic performance and effectiveness of a mini shell and tube heat exchanger working with a nanofluid regarding effects of fins and nanoparticle shape. *Adv. Powder Technol.* **32**(12), 4468–4480. <https://doi.org/10.1016/J.APT.2021.09.042> (2021).
41. Mazaheri, N., Bahiraei, M. & Razi, S. Second law performance of a novel four-layer microchannel heat exchanger operating with nanofluid through a two-phase simulation. *Powder Technol.* **396**, 673–688. <https://doi.org/10.1016/J.POWTEC.2021.11.021> (2022).
42. Bahiraei, M. & Monavari, A. Irreversibility characteristics of a mini shell and tube heat exchanger operating with a nanofluid considering effects of fins and nanoparticle shape. *Powder Technol.* **398**, 117117. <https://doi.org/10.1016/J.POWTEC.2022.117117> (2022).
43. Bahiraei, M., Mazaheri, N. & Hanooni, M. Employing a novel crimped-spiral rib inside a triple-tube heat exchanger working with a nanofluid for solar thermal applications: Irreversibility characteristics. *Sustain. Energy Technol. Assessments* **52**, 102080. <https://doi.org/10.1016/J.SETA.2022.102080> (2022).
44. Schateva, M., Ficko, M. & Kostić, S. The characteristics and applications of synthetic lubricating greases. *J. Synth. Lubr.* **3**(2), 83–92. <https://doi.org/10.1002/JSL.3000030202> (1986).
45. Narumanchi, S., Mihalic, M., Kelly, K. & Eesley, G. Thermal interface materials for power electronics applications. In *2008 11th IEEE Intersoc. Conf. Therm. Thermomechanical Phenom. Electron. Syst. I-THERM* 395–404 (2008). <https://doi.org/10.1109/ITHERM.2008.4544297>.
46. Paszkowski, M. Assessment of the effect of temperature, shear rate and thickener content on the thixotropy of lithium lubricating greases. *Proc. Inst. Mech. Eng. Part J J. Eng. Tribol.* **227**(3), 209–219. <https://doi.org/10.1177/1350650112460950> (2012).
47. Zhou, Y., Bosman, R. & Lugt, P. M. A master curve for the shear degradation of lubricating greases with a fibrous structure. *Tribol. Trans.* **62**(1), 78–87. <https://doi.org/10.1080/10402004.2018.1496304> (2018).
48. Fan, X., Xia, Y. & Wang, L. Tribological properties of conductive lubricating greases. *Friction* **2**(4), 343–353. <https://doi.org/10.1007/s40544-014-0062-2> (2014).
49. Dresel, W. & Heckler, R.-P. Lubricating greases. *Lubr. Lubr.* **2017**, 781–842. <https://doi.org/10.1002/9783527645565.CH16> (2017).
50. Salah, F., Aziz, Z. A. & Ching, D. L. C. New exact solution for Rayleigh-Stokes problem of Maxwell fluid in a porous medium and rotating frame. *Results Phys.* **1**(1), 9–12. <https://doi.org/10.1016/J.RINP.2011.04.001> (2011).
51. Khalid, A., Khan, I., Khan, A. & Shafie, S. Unsteady MHD free convection flow of Casson fluid past over an oscillating vertical plate embedded in a porous medium. *Eng. Sci. Technol. Int. J.* **18**(3), 309–317. <https://doi.org/10.1016/j.jestch.2014.12.006> (2015).
52. Atangana, A. Fractal-fractional differentiation and integration: Connecting fractal calculus and fractional calculus to predict complex system. *Chaos Solitons Fract.* **102**, 396–406. <https://doi.org/10.1016/J.CHAOS.2017.04.027> (2017).
53. Khalid, A., Khan, I. & Shafie, S. Exact solutions for free convection flow of nanofluids with ramped wall temperature. *Eur. Phys. J. Plus* **130**(4), 1–14. <https://doi.org/10.1140/EPJP/I2015-15057-9> (2015).

### Author contributions

N.K. solved the problem, F.A. model the problem and performed transformations, N.K and Z.A. data analysis, Z.A and S.M. discussed results, A.H.G. performed numerical simulations, N.K and I.K. computed results, software, coding, S.M.E. computed results as special cases, comparison, results discussion, manuscript revision.

### Competing interests

The authors declare no competing interests.

### Additional information

**Correspondence** and requests for materials should be addressed to F.A.

**Reprints and permissions information** is available at [www.nature.com/reprints](http://www.nature.com/reprints).

**Publisher's note** Springer Nature remains neutral with regard to jurisdictional claims in published maps and institutional affiliations.



**Open Access** This article is licensed under a Creative Commons Attribution 4.0 International License, which permits use, sharing, adaptation, distribution and reproduction in any medium or format, as long as you give appropriate credit to the original author(s) and the source, provide a link to the Creative Commons licence, and indicate if changes were made. The images or other third party material in this article are included in the article's Creative Commons licence, unless indicated otherwise in a credit line to the material. If material is not included in the article's Creative Commons licence and your intended use is not permitted by statutory regulation or exceeds the permitted use, you will need to obtain permission directly from the copyright holder. To view a copy of this licence, visit <http://creativecommons.org/licenses/by/4.0/>.

© The Author(s) 2023